Inorganic Chemistry

ARTICLE

pubs.acs.org/IC

Spectroscopic and Computational Studies of Glutathionylcobalamin: Nature of Co−S Bonding and Comparison to Co−C Bonding in Coenzyme B_{12}

Karen S. Conrad and Thomas C. Brunold*

Department of Chemistry, University of Wisconsin—Madison, Madison, Wisconsin 53706, United States

Supporting Information

ABSTRACT: Glutathionylcobalamin (GSCbl) is a unique, biologically relevant cobalamin featuring an axial Co−S bond that distinguishes it from the enzymatically active forms of vitamin B_{12}, which possess axial Co−C bonds. GSCbl has been proposed to serve as an intermediate in cobalamin processing and, more recently, as a therapeutic for neurological disorders associated with oxidative stress. In this study, GSCbl and its close relative cysteinylcobalamin (CysCbl) were investigated using electronic absorption, circular dichroism, magnetic circular dichroism, and resonance Raman spectroscopies. The spectroscopic data were analyzed in the framework of density functional theory (DFT) and time-dependent DFT computations to generate experimentally validated electronic structure descriptions. Although the change in the upper axial ligand from an alkyl to a thiol group represents a major perturbation in terms of the size, basicity, and polarizability of the coordinating atom, our spectroscopic and computational results reveal striking similarities in electronic structure between methylcobalamin (MeCbl) and GSCbl, especially with regard to the σ donation from the alkyl/thiol ligand and the extent of mixing between the cobalt 3d and the ligand frontier orbitals. A detailed comparison of Co−C and Co−S bonding in MeCbl and GSCbl, respectively, is presented, and the implications of our results with respect to the proposed biological roles of GSCbl are discussed.

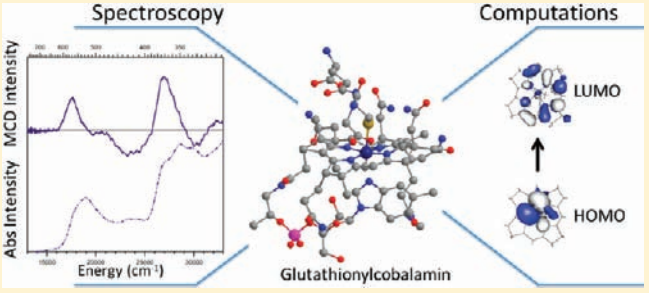

1. INTRODUCTION

Vitamin B_{12} and its derivatives, known as cobalamins (Cbls),[1] are among Nature's most complex cofactors. Cbls have been the subject of intense investigation since vitamin B_{12} was first isolated in 1948 in the laboratories of Folkers[2] and Smith[3,4] and structurally characterized in 1956 in the laboratory of Dorothy Hodgkin.[5−11] These species contain a central low-spin Co^{3+} ion ligated equatorially by four nitrogens of a tetrapyrollic corrin ring and coordinated axially in the lower (α) position by a N atom of a 5,6-dimethylbenzimidazole (DMB) base that is attached to the corrin ring via a nucleotide loop and in the upper (β) position by a variable ligand X (e.g., X = CH_3 in methylcobalamin (MeCbl), 5′-deoxyadenosyl in adenosylcobalamin (AdoCbl), H_2O in aquocobalamin (H_2OCbl^+), CN^- in cyanocobalamin or vitamin B_{12}, and L-glutamyl-L-cysteinylglycine, GS^-, in glutathionylcobalamin (GSCbl); see Figure 1).[6] Cbl is found in animals and bacteria, and it is an essential nutrient for humans because they lack the enzyme machinery for its biosynthesis. However, Cbl is biosynthesized via both aerobic and anaerobic pathways in select archaea and bacteria.[5,10,12−15]

MeCbl and AdoCbl are the enzymatically active forms of the cofactor required by humans for catalysis in methionine synthase (MetH)[16,17] and methylmalonyl-CoA mutase (MMCM),[18] respectively. MeCbl-dependent enzymes like MetH catalyze methyl-transfer reactions in which the Co−C bond of the cofactor is cleaved heterolytically.[16,19,20] Alternatively, AdoCbl-dependent enzymes include two classes of isomerases that catalyze rearrangement reactions via homolytic cleavage of the cofactor's Co−C bond.[21−24] Cbl deficiency in humans caused by improper diet, a lack of proper Cbl adsorption, and/or inborn errors in processing Cbl leads to a variety of adverse conditions, most notably the disorders of megaloblastic anemia and homocystinuria for errors in MeCbl processing and methylmalonic aciduria for errors in AdoCbl processing.[25−27] In humans the MeCbl-dependent MetH and AdoCbl-dependent MMCM are located in different intracellular locales, the cytosol and the mitochondrial matrix, respectively. Thus, the intracellular trafficking of Cbl is critical to maintaining functional MetH and MMCM and has been under intensive investigation.[25,28−31]

Glutathione (GSH) is a γ-glutamylcysteinylglycine tripeptide featuring an unusual peptide linkage between the COO^- side chain of glutamate and the $-NH_2$ group of cysteine. One of the major roles of GSH in vivo is redox regulation in the intracellular milieu.[32,33] It plays additional roles in the biosynthesis of sulfur-containing metabolites, metabolism regulation, and protection

Received: March 2, 2011
Published: August 22, 2011

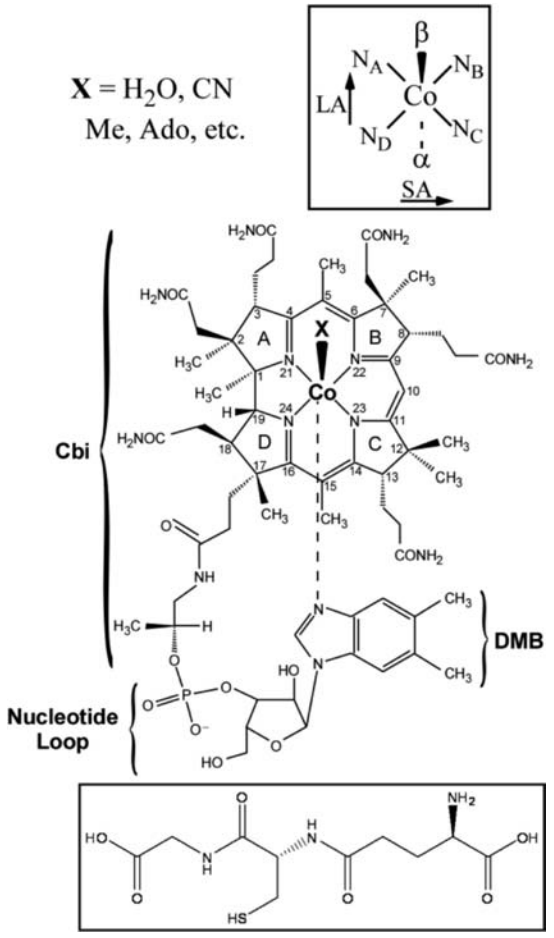

Figure 1. Chemical structure and numbering scheme used to identify the relevant C and N atoms of the corrin ring of Co^{3+}Cbl, where X denotes the variable upper axial ligand. (Inset top) Upper (β) and lower (α) faces of the cofactor and orientation of the long axis (LA) and short axis (SA) of the corrin ring. (Inset bottom) Chemical structure of glutathione.

against free radical damage.[34,35] GSH has been reported to reach concentrations of up to 10 mM in cells.[36] In the presence of GSH, H_2OCbl^+ is rapidly and irreversibly converted to GSCbl via β-ligand exchange, with a half-life for formation of 2.8 s at 37 °C and ~5 mM concentrations of GSH.[37] Thus, any free H_2OCbl^+ in the cell lacking protection from a protein chaperone or cellular organelle is susceptible to conversion to GSCbl, though the fraction of free intracellular Cbl is estimated to be less than 5%.[38]

The physiological significance of GSCbl was initially suggested by Wagner and Bernhauer in 1964[39] and established more fully by enzymatic studies completed by Jacobsen and co-workers in 1990.[40] GSCbl and sulfitocobalamin (X = SO_3^{2-} in Figure 1) are the two sulfur-containing Cbls that have been extracted from cultured endothelial cells and shown to be naturally occurring, as opposed to resulting from the extraction process.[41] Cysteinylcobalamin (CysCbl) is another thiolatocobalamin, but compared to GSCbl it is relatively unstable, readily decomposing into a thiyl radical and Co^{2+}Cbl.[42−45] The decreased stability of CysCbl over GSCbl was attributed to the destabilizing effect of the charged $-NH_3^+$ group of Cys on the Co−S bond.[42] GSCbl has an amide bond in the place of the $-NH_3^+$ group of Cys; additionally, the larger size of GS^- may enable formation of favorable interactions between the terminal carboxylates and the corrin side chains, thereby increasing the stability of GSCbl. The precise role of GSCbl in vivo is still unclear, but due to its natural occurrence it has been proposed to be an intermediate in the biosynthesis of AdoCbl and MeCbl, two pathways that continue to be the subject of intense research.[40,41,46]

More recently, GSCbl has been identified as a promising intracellular antioxidant,[46] being nontoxic at concentrations exceeding 2 mM. GSCbl is able to inhibit intracellular peroxide production and prevent apoptotic and necrotic cell death in vitro more efficiently than other forms of Cbl.[46] Originally proposed to be used as a treatment for Alzheimer's by McCaddon et al. in 2002, GSCbl has continued to show promise for the treatment of conditions with associated inflammatory oxidative stress, including dementia, arthritis, and cancer.[47,48] GSCbl has also been shown to promote MetH activity much more effectively than CNCbl or H_2OCbl^+.[40] What remains to be elucidated is why GSCbl is more effective than any other Cbl in these roles and how exactly GS^- impacts the intracellular processing of free Cbl.

In this study we used electronic absorption (Abs), circular dichroism (CD), magnetic CD (MCD), and resonance Raman (rR) spectroscopic techniques to characterize GSCbl and CysCbl. To complement the experimental data, quantum mechanics/molecular mechanics (QM/MM) geometry optimizations of entire cofactor models were performed and the optimized structures were used for density functional theory (DFT) calculations to generate experimentally validated geometric and electronic structure descriptions. Additionally, time-dependent DFT (TDDFT) calculations were employed to assign the key electronic transitions that contribute to the Abs, CD, and MCD spectra of GSCbl. Although GSCbl had been the subject of previous investigations using DFT calculations[49,50] and X-ray absorption spectroscopy,[51−53] the similarities and differences in the electronic structures of GSCbl and other Cbls and the role that the unique Co−S bond plays in modulating the properties of GSCbl have remained largely unexplored. By comparing our results for GSCbl to those reported previously for MeCbl, unique insight has been obtained into the similarities and differences between the Co−S and Co−C bonding interactions in thiolatocobalamins and alkylcobalamins, respectively.

2. EXPERIMENTAL AND COMPUTATIONAL METHODS

Synthesis. Glutathione, cysteine, [H_2OCbl]Cl, and MeCbl were purchased from Sigma and used without further purification. GSCbl and CysCbl were prepared according to published procedures.[40] Samples for low-temperature Abs, CD, and MCD spectroscopic experiments were prepared in 60% (v/v) glycerol. Samples for low-temperature rR spectroscopic experiments were prepared as pellets either by injecting aqueous solutions of the Cbl of interest into $N_{2(l)}$ or by dissolving solid Cbl in H_2O before adding glycerol and injecting the solutions into $N_{2(l)}$.

Spectroscopy. Abs, CD, and MCD spectra were obtained using a Jasco J-715 spectropolarimeter in conjunction with an Oxford Instruments SM-4000 8T magnetocryostat. All MCD spectra reported herein were obtained by subtracting the −7 T spectrum from the +7 T spectrum to eliminate contributions from the natural CD. Sample concentrations were determined spectrophotometrically at 300 K using a Varian Cary 5E UV−vis−NIR spectrophotometer and published molar extinction coefficients.[45,54,55]

rR spectra were obtained upon excitation with a Coherent I-305 Ar^+ ion laser or a Coherent I-302C Kr^+ ion laser with ~10−20 mW of laser power at the sample. The scattered light was collected using a ~135° backscattering arrangement, dispersed by an Acton Research triple

monochromator equipped with 1200 and 2400 grooves/mm gratings, and analyzed with a Princeton Instruments Spec X: 100BR deep depletion, back-thinned CCD camera. rR data were collected at 77 K on frozen pellets situated directly in an EPR dewar filled with $N_{2(l)}$ to prevent photodegradation.

Computations. *Geometry Optimization.* Models of GSCbl and MeCbl for computational studies were generated by quantum mechanics/molecular mechanics (QM/MM) geometry optimizations starting from the high-resolution X-ray crystal structures of GluCysCbl and MeCbl (XIQSEV and WIKXOD, respectively).[42,49] For the GSCbl model, the free GSH ligand was geometry optimized separately using DFT methods before appending it to the cobalt ion in place of the GluCys ligand contained in the XIQSEV structure. In each case the corrin ring, the benzimidazole lower axial ligand, and the first atom of the upper axial ligand were included in the QM region, while the remainder of the model was treated with MM. All geometry optimizations were carried out on a cluster of 10 Pentium Xeon nodes (Ace computers) employing the Amsterdam Density Functional (ADF) 2008.01 suite of programs with an integration parameter of 5.0 and the TZP basis set with a frozen core through 1s (C, N, O) or 2p (Co, P, S).[56−58] The geometry convergence criteria chosen were 0.0001 hartree in the total energy, 0.001 hartree/Å in the Cartesian gradients, and 0.001 Å in the estimated uncertainty of the Cartesian coordinates. The density functional utilized was composed of the Vosko, Wilk, and Nusair-5 local density approximation and the Perdew−Burke−Ernzerhof generalized gradient approximation for exchange and correlation.[59,60]

Single-Point DFT and TDDFT Calculations. The ORCA 2.6.35 software package, developed by Dr. Frank Neese (Universität Bonn, Germany),[61] was used to perform single-point DFT and TDDFT calculations on suitably truncated models of GSCbl and MeCbl, derived from their respective QM/MM geometry-optimized model. In each case, Becke's three-parameter hybrid functional for exchange[62,63] was used along with the Lee−Yang−Parr correlation functional[64] (B3LYP). The TZVP basis set[65] was chosen for Co and all atoms bound directly to Co, while the VDZ/P basis set[66] (Ahlrichs split valence set with one set of first polarization functions on all atoms) was used in conjunction with the SV/C auxiliary basis set for the remaining atoms. A total of 60 excited states were calculated with TDDFT by considering all single excitations between molecular orbitals (MOs) with orbital energies within a window of ±3 hartree around the highest occupied MO and lowest unoccupied MO (HOMO/LUMO) gap. To assist in the interpretation and assignment of key electronic transitions, isosurface plots of the MOs and electron density difference maps (EDDMs) were generated with the gOpenMol program[67−69] using isodensity values of 0.03 and 0.003 au, respectively. To compare the computational data with our experimental Abs spectra of GSCbl and MeCbl, the TDDFT results were used to compute Abs traces by modeling each predicted transition as a Gaussian band with a full width at half-maximum of 1700 cm^{-1}.[70]

3. RESULTS AND ANALYSIS

3.1. Spectroscopic Results for GSCbl, CysCbl, and MeCbl. *(i). Abs, CD, and MCD Data.* The Abs, CD, and MCD spectra of GSCbl, CysCbl, and MeCbl obtained at 280 K are shown in Figure 2. As expected, the data sets of the two thiolatocobalamins are nearly identical. The color variation of the complexes from pink (MeCbl) to deep purple (GSCbl, CysCbl) correlates with a red shift of the prominent low-energy Abs feature, the so-called α/β bands. This red shift (by ∼400 cm^{-1}) is even more evident in the corresponding MCD spectra, owing to the increased resolution of the spectral features in these spectra. A detailed analysis of the MeCbl Abs, CD, and MCD data was presented in a previous publication from this laboratory[71] and will be used here

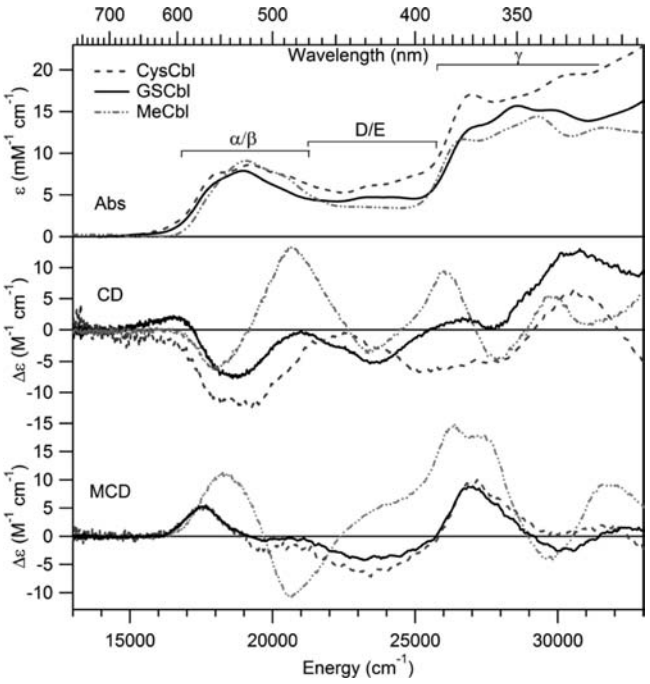

Figure 2. Abs (top), CD (center), and 7 T MCD (bottom) spectra at 280 K of GSCbl (−), CysCbl (---), and MeCbl (−·−). The different regions of the Abs spectra are highlighted.

as the basis for a comparison with the results obtained in this study for the thiolatocobalamins. The α and β bands in the low-energy region of the MeCbl Abs spectrum were assigned to the origin and first member of a vibronic progression associated with a single electronic transition originating from the corrin π-based HOMO and terminating in the corrin π*-based LUMO. The energy of this transition was found to vary markedly as a function of the upper axial ligand, as the σ-donor strength of this ligand modulates the Co $3d_{z2}$ orbital character in the HOMO and, thus, the strength of the σ-antibonding interaction between the Co ion and lower axial base in this MO. Consequently, the fact that the α/β bands appear at nearly the same energies in the Abs spectra of MeCbl and the thiolatocobalamins implies that the Co−C and Co−S σ-bonding interactions are quite similar in nature.

Toward higher energy, the three bands in the D/E region (∼22 000−26 000 cm^{-1}) of the MeCbl Abs spectrum are conserved in the GSCbl and CysCbl Abs spectra with minimal (<200 cm^{-1}) energy shifts, though their signs and intensities within the CD and MCD spectra vary considerably among the three species. In the high-energy γ region (26 000−33 000 cm^{-1}), the number and energies of the discernible features are essentially the same for each species but the relative band intensities again vary quite substantially. Our previous analysis of the MeCbl Abs spectrum revealed that the electronic transitions producing the dominant contributions to the γ region include corrin-centered π → π* and, to a lesser extent, Co 3d → corrin π* charge transfer excitations with varying polarizations. Hence, small differences in the charge donation of the axial thiolate and alkyl ligands to the Co center likely account for the observed spectral variations in this region.

The GSCbl and MeCbl Abs and MCD spectra were iteratively fit with the fewest acceptable number of Gaussian bands to resolve the major electronic transitions contributing to each data set and to quantify the key differences between them.

dx.doi.org/10.1021/ic200428r |Inorg. Chem. 2011, 50, 8755–8766

These spectral deconvolutions (Figure 3 and Table 1) indicate that at least 14 bands contribute to the MeCbl and GSCbl spectra in the region below 34 000 cm^{-1}. The α/β region of the GSCbl MCD spectrum is dominated by a positively signed band centered at 17 470 cm^{-1}, with two less intense bands at 16 000 and 18 700 cm^{-1} also contributing to this region. In contrast, the α/β region of the MeCbl MCD spectrum is fit with two positively signed bands of almost equal intensity, previously identified as the origin and first vibronic sideband associated with the corrin-based HOMO → LUMO (i.e., corrin $\pi \rightarrow \pi^*$) transition, as well as two negatively signed bands centered at 20 550 and 21 800 cm^{-1} (bands 3 and 4, Table 1) that were attributed to members of a vibrational progression associated with another corrin-based $\pi \rightarrow \pi^*$ transition. The bands contributing to the γ region of the MeCbl spectra (i.e., above 26 000 cm^{-1}) were shown previously to arise from at least four distinct electronic transitions with significant corrin $\pi \rightarrow \pi^*$ character. Because essentially the same set of bands is present in the GSCbl spectra, we conclude that these spectra also contain contributions from at least four corrin-based $\pi \rightarrow \pi^*$ transitions in the γ region.

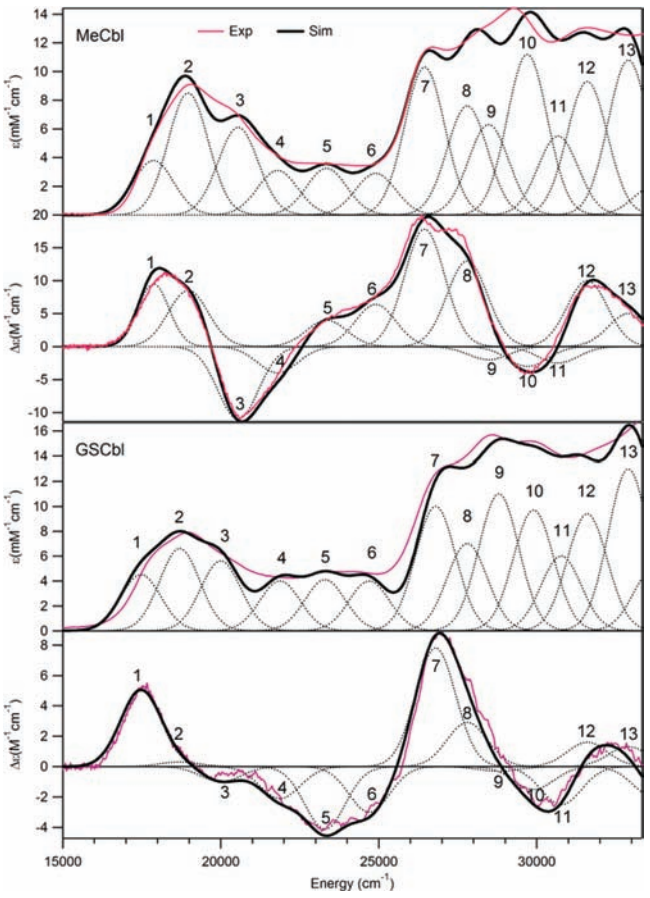

Figure 3. Solid red lines: 280 K Abs and 7 T MCD spectra of MeCbl (top) and GSCbl (bottom). Dotted black lines: Gaussian deconvolutions of the experimental spectra. Solid black lines: Overall fits obtained by taking the sum of the individual Gaussian bands.

(ii). Resonance Raman Data. Figure 4A shows the rR spectra of frozen aqueous solutions of MeCbl, GSCbl, and CysCbl obtained with 568.2 nm (17 599 cm^{-1}) laser excitation, corresponding to the low-energy tail of the α/β bands in the corresponding Abs spectra. Previous rR studies of MeCbl identified two strongly enhanced features that were assigned as corrin-based vibrational modes polarized along the short axis, ν_{SA} (a corrin mode primarily involving C═C stretching motion along the $C_5\cdots C_{15}$ vector, see Figure 1), at 1543 cm^{-1} and the long axis, ν_{LA} (which mainly involves C═C stretching motion along the $Co\cdots C_{10}$ vector), at 1490 cm^{-1}, as well as a weak feature associated with the Co−C stretching mode, ν_{Co-C}, at 504 cm^{-1}.[71] While ν_{LA} and ν_{Co-C} are predominantly enhanced for excitation in resonance with the corrin-based HOMO → LUMO transition (the α/β region), ν_{SA} displays the largest enhancement for excitation in the γ region. Since the dominant features in the rR spectra of Cbls are due primarily to corrin vibrations, the rR spectra of MeCbl, GSCbl, and CysCbl are very similar. Specifically, in the spectra obtained with 568.2 nm excitation, the dominant feature, corresponding to ν_{LA}, occurs within 5 cm^{-1} for the three cofactors. However, in the low-energy region where Co−ligand vibrations are expected

Table 1. Fit Parameters from Gaussian Deconvolution of the Abs and MCD Spectra of MeCbl (left) and GSCbl (right) Shown in Figure 3

	MeCbl			GSCbl		
band	energy	ε (Abs) (mM^{-1} cm^{-1})	$\Delta\varepsilon$ (MCD) (M^{-1} cm^{-1})	energy	ε (Abs) (mM^{-1} cm^{-1})	$\Delta\varepsilon$ (MCD) (M^{-1} cm^{-1})
1	17 870	3.8	9.5	17 470	3.1	6.5
2	18 970	8.5	8.5	18 700	6.6	0.3
3	20 550	6.1	−11	20 000	5.6	−1
4	21 800	3.1	−4	21 875	4	−2.1
5	23 350	3.25	4	23 300	4.1	−4.1
6	24 900	2.9	6.4	24 700	4	−3
7	26 450	10.3	17.8	26 800	10	7.8
8	27 800	7.6	13	27 800	7	2.9
9	28 475	6.3	−2	28 800	11	−0.3
10	29 700	11.2	−3	29 900	9.7	−1.5
11	30 675	5.5	−2.5	30 775	6	−2.5
12	31 600	9.3	10	31 600	9.4	1.6
13	32 900	10.8	5	32 900	13	1.3
14	33 700	2	0	33 700	5	−2

dx.doi.org/10.1021/ic200428r |*Inorg. Chem.* 2011, 50, 8755–8766

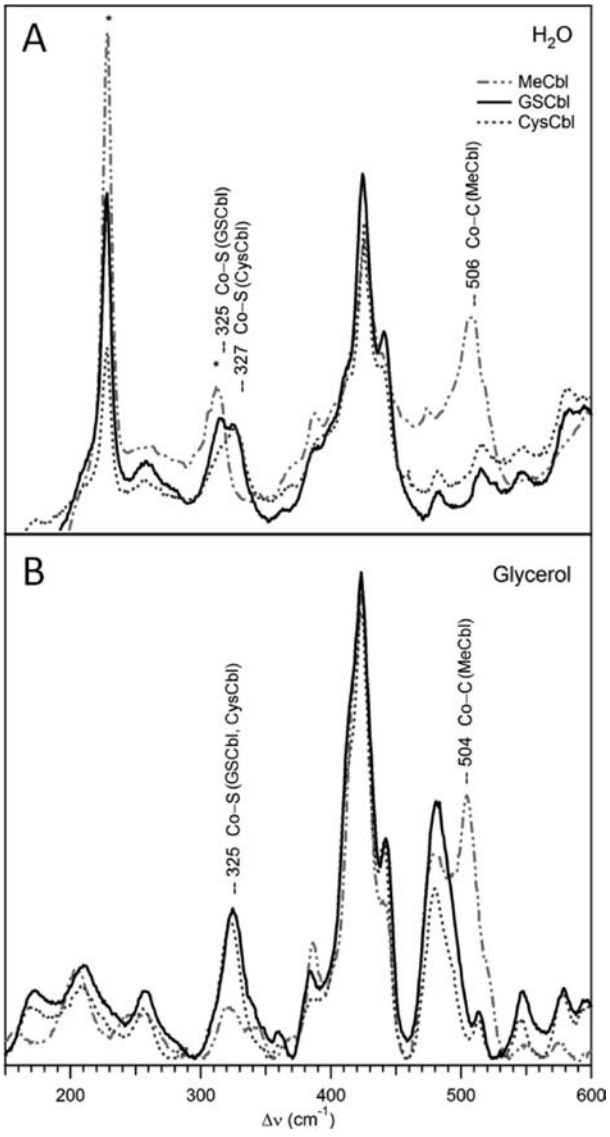

Figure 4. rR spectra at 77 K of MeCbl (– · ·), GSCbl (—), and CysCbl (---) in frozen aqueous solution (A) and a ∼90% v/v mixture of glycerol and water (B) obtained with 568.2 nm (17 599 cm^{-1}) laser excitation. Ice peaks are marked with asterisks, and the positions of the Co−C and Co−S stretches are indicated.

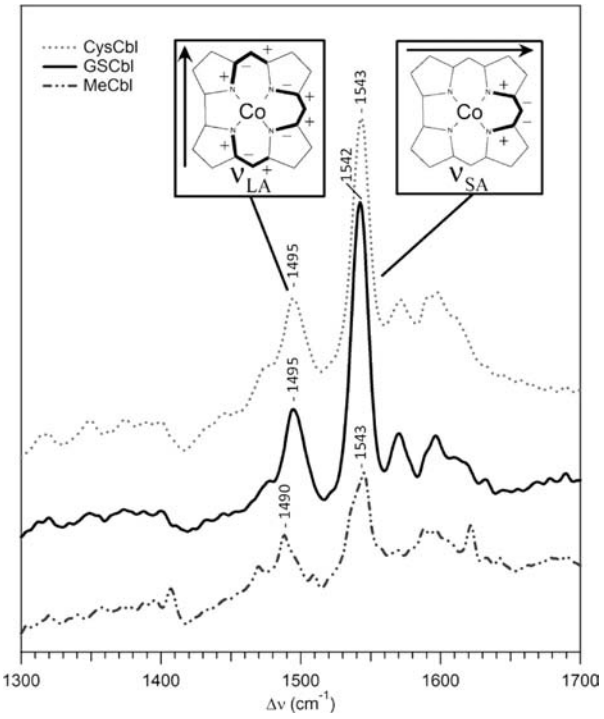

Figure 5. rR spectra at 77 K of CysCbl (---), GSCbl (—), and MeCbl (– · ·–) in frozen aqueous solution obtained with 363.8 nm (27 488 cm^{-1}) laser excitation. (Insets) Depictions of the corrin-based symmetric long-axis (ν_{LA}) and short-axis (ν_{SA}) stretching modes (the + and − signs indicate bond elongations and contractions, respectively).

to occur, the GSCbl and CysCbl rR spectra exhibit features at 325 and 327 cm^{-1}, respectively, that have no counterpart in the MeCbl spectrum.

Because features due to vibrations of the ice lattice occur in the same spectral region as, and overlap with, the Co−ligand vibrational modes of interest, rR data were also obtained for frozen samples containing glycerol (Figure 4B). In these spectra the Co−C stretch for MeCbl appears at 504 cm^{-1}, while the Co−S stretches (ν_{Co-S}) of both GSCbl and CysCbl can now be clearly discerned at 325 cm^{-1}. The increased mass of the coordinated S atom of the GS$^-$ ligand, relative to that of the C atom of the CH_3 ligand in MeCbl, is expected to downshift the ν_{Co-S} stretch by 157 cm^{-1} from the ν_{Co-C} stretch, which accounts for most of the experimentally determined shift of 179 cm^{-1}. The fact that the ν_{Co-S} stretch is resonance enhanced for laser excitation at λ_{ex} = 568.2 nm (17 599 cm^{-1}), which corresponds to the energy of the corrin-based HOMO → LUMO transition, indicates that the Co−S bond and corrin π system of GSCbl are electronically coupled in a similar manner as the Co−C bond and corrin π system of MeCbl.[71−73]

rR spectra of MeCbl, GSCbl, and CysCbl obtained with λ_{ex} = 363.8 nm (27 488 cm^{-1}) are presented in Figure 5. Laser excitation in this higher energy spectral region, where corrin $\pi \rightarrow \pi^*$ transitions polarized along the Co···C_{10} vector occur, gives rise to predominant enhancement of ν_{SA}.[74] As shown in Figure 5, the ν_{SA} modes of MeCbl, GSCbl, and CysCbl invariably peak at ∼1543 cm^{-1}. According to a previous study, the frequency of ν_{SA} decreases with decreasing positive charge of the central Co ion.[75] For example, the ν_{SA} frequency for H_2OCbl^+ is 1543 cm^{-1}, while for Co^{2+}Cbl it is 1509 cm^{-1}, and for Co^{1+}Cbl it is 1487 cm^{-1} (Table S1, Supporting Information). From this comparison, it appears that the alkyl and thiol ligands donate essentially the same amount of electron density to the Co^{3+} ion, consistent with the similar α/β band positions in the Abs spectra of MeCbl, GSCbl, and CysCbl (vide supra).

3.2. Computational Results. *(i). Geometry-Optimized Models.* Models of GSCbl and MeCbl were generated by carrying out quantum mechanics/molecular mechanics (QM/MM) geometry optimization starting from suitably chosen X-ray crystal structures (see section 2). Overall, the optimized models (Figure 6) exhibit only small differences from these crystal-structure data, and their Co−N_{corrin}, Co−N_{DMB}, and Co−X_{ax} bond lengths and corrin fold angles also agree well with those obtained from X-ray structural studies of related Cbls.[42,51−53] The most notable difference between the optimized models and the crystal structure-based input geometries involves a moderate flattening of the corrin ring, as revealed by a decrease in the corrin

dx.doi.org/10.1021/ic200428r |*Inorg. Chem.* 2011, 50, 8755–8766

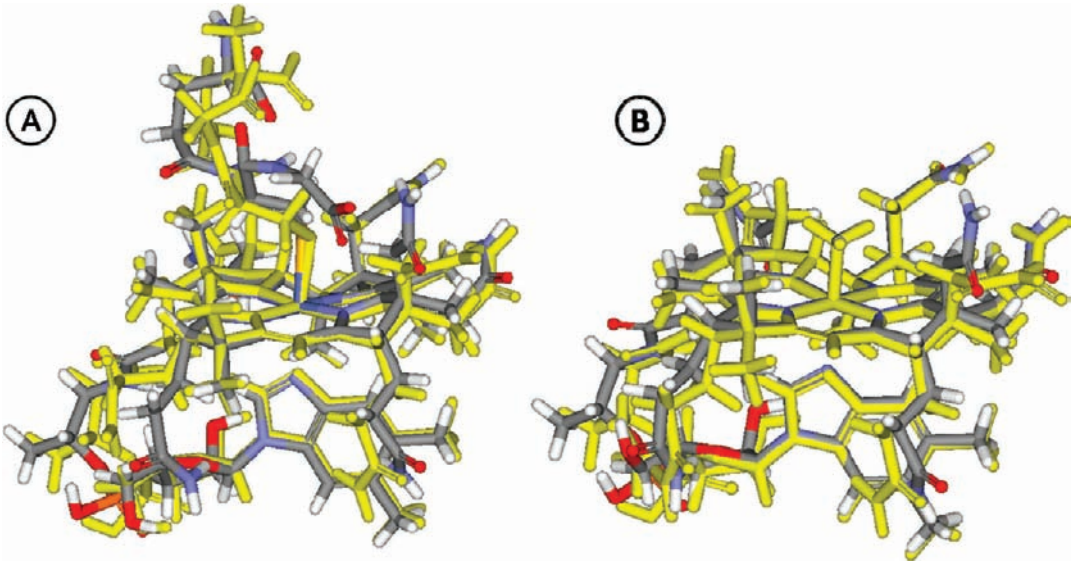

Figure 6. QMMM-optimized models (yellow) of GSCbl (A) and MeCbl (B) overlaid on X-ray crystal structure-based input models (colored by atom).

fold angles along the $C_5\cdots C_{15}$ vector (θ) and along the $Co\cdots C_{10}$ vector (ϕ) by 4−8° (Table S2, Supporting Information). The axial $Co-N_{DMB}$ and Co−S bond lengths of GSCbl decreased by 0.01 and 0.07 Å, respectively, during the QM/MM geometry optimization, possibly due to removal of constraints imposed by crystal packing. In contrast, in the case of MeCbl, both the $Co-N_{DMB}$ and the Co−C axial bond lengths increased slightly, by 0.09 and 0.01 Å, respectively. Other noticeable changes during the optimization process were mostly contained within the MM region and included some movement of the nucleotide loop and pendant side chains on the corrin mostly at distances > 6 Å from the Co center. Despite these minor differences between the QM/MM-optimized models and the X-ray crystal-structure data, the optimized models nicely reproduce the essential features of the experimental structures and were thus considered acceptable for use in further calculations.

(ii). TDDFT Results. TDDFT calculations were carried out on truncated derivatives of the QM/MM-optimized cofactor models that included the corrin ring, an imidazole in the lower axial position, the entire methyl group for MeCbl and $-SCH_3$ instead of glutathione for GSCbl in the upper axial position, and hydrogen atoms in place of the corrin side chains at bond lengths reduced by 30%. Simulated Abs spectra were generated from the TDDFT results using a Gaussian convolution function with a full width at half-maximum of 1700 cm^{-1} and by applying a uniform red shift of 3000 cm^{-1} to compensate for the tendency of the B3LYP hybrid functional to overestimate transition energies.[62,63]

The TDDFT-computed Abs spectra for MeCbl and GSCbl (Figure 7, Tables 2 and 3) correctly predict the number, energies, and relative intensities of the transitions responsible for the main spectral features observed experimentally. In the case of MeCbl, our TDDFT results also agree well with those obtained previously from calculations using the unoptimized crystal-structure geometry.[71] As required by the rR spectra presented above and published rR excitation profile data for MeCbl,[71] TDDFT predicts the lowest-energy transition responsible for the α/β band to be polarized along the $C_5\cdots C_{15}$ vector (i.e., corrin long axis) and the transitions in the γ region to be polarized primarily along the $Co\cdots C_{10}$ vector (corrin short axis).

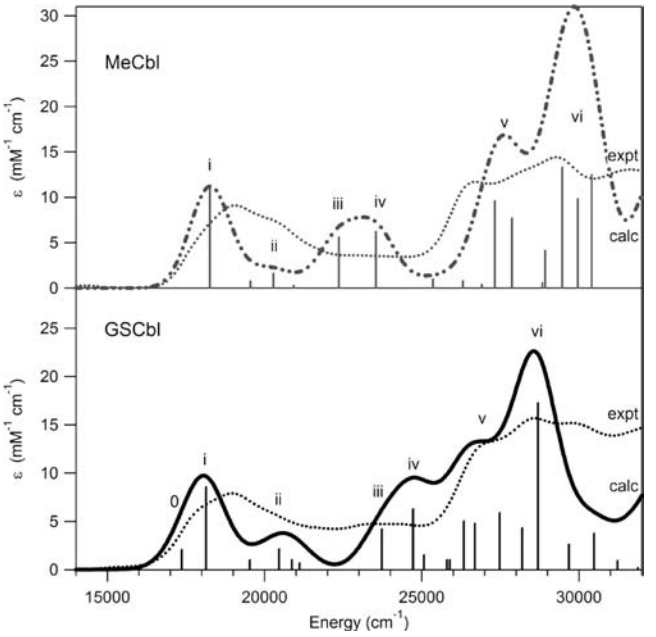

Figure 7. Experimental (280 K) and TDDFT-computed Abs spectra for MeCbl and GSCbl. The calculated spectra were uniformly red shifted by 3000 cm^{-1} to facilitate a direct comparison with the experimental data. The major bands in the calculated spectra are labeled, and the transitions producing the dominant contributions are indicated by vertical solid lines.

(iii). DFT-Computed MO Diagrams. The satisfactory agreement between the TDDFT-computed and the experimental Abs spectra of MeCbl and GSCbl warrants a more detailed analysis of the DFT-calculated MO descriptions for these models. Isosurface plots of the relevant MOs of MeCbl (left) and GSCbl (right) are presented in Figure 8. The corrin ring is a strongly σ- and moderately π-donating tetradentate equatorial ligand; consequently, the Co $3d_{xy}$-based MO (MeCbl MO#121, GSCbl MO#128) is strongly σ-antibonding with respect to the Co−N(corrin) bonds and thus unoccupied, whereas the Co $3d_{x2-y2}$-based MO (MeCbl MO#111, GSCbl MO#118) is essentially nonbonding

dx.doi.org/10.1021/ic200428r |*Inorg. Chem.* 2011, 50, 8755–8766

Table 2. TDDFT-Calculated Energies (in cm^{-1}), Polarizations, Oscillator Strengths, and Percent Contributions from One-Electron Excitations for the Major Electronic Transitions of MeCbl (band designations relate to Figure 7)

band	state	E (cm^{-1})	polarization	f	transition	%	donor MO	acceptor MO
i	1	18 260	LA	0.0767	116 → 117	85	cor-π (HOMO)	cor-π^* (LUMO)
ii	3	20 288	LA	0.0111	115 → 121	20	Co $3d_{yz}$/cor-π (HOMO-1)	Co $3d_{xy}$
					110 → 121	14	Co $3d_{yz}/3d_{x2-y2}$	Co $3d_{xy}$
					114 → 121	12	Co $3d_{xz}$	Co $3d_{xy}$
iii	5	22 367	SA	0.0388	115 → 117	64	Co $3d_{yz}$/cor-π (HOMO-1)	cor-π^* (LUMO)
					116 → 118	21	cor-π	cor-π^* (LUMO+1)
iv	6	23 541	LA	0.0431	114 → 117	78	Co $3d_{xz}$	cor-π^* (LUMO)
v	10	27 326	SA	0.0664	116 → 121	30	cor-π	Co $3d_{xy}$
					116 → 118	28	cor-π	cor-π^* (LUMO+1)
					110 → 117	10	Co $3d_{yz}/3d_{x2-y2}$	cor-π^* (LUMO)
	11	27 866	SA	0.0531	111 → 117	31	Co $3d_{x2-y2}/3d_{yz}$	cor-π^* (LUMO)
					116 → 118	23	cor-π	cor-π^* (LUMO+1)
					115 → 118	11	Co $3d_{yz}$/cor-π (HOMO-1)	cor-π^* (LUMO+1)
					116 → 121	10	cor-π	Co $3d_{xy}$
vi	13	28 930	SA	0.0286	111 → 117	23	Co $3d_{x2-y2}/3d_{yz}$	cor-π^* (LUMO)
					110 → 117	21	Co $3d_{yz}/3d_{x2-y2}$	cor-π^* (LUMO)
					114 → 121	13	Co $3d_{xz}$	Co $3d_{xy}$
	14	29 473	LA	0.0919	112 → 117	35	Co $3d_{z2}/3d_{yz}$	cor-π^* (LUMO)
					115 → 118	24	Co $3d_{yz}$/cor-π (HOMO-1)	cor-π^* (LUMO+1)
					116 → 119	10	cor-π	cor/ligand-π^*
	15	29 968	SA	0.0680	116 → 119	34	cor-π	cor/ligand-π^*
					116 → 120	32	cor-π	Co $3d_{z2}$/cor-π^*
	16	30 407	SA	0.0861	114 → 118	16	Co $3d_{xz}$	cor-π^* (LUMO+1)
					111 → 119	11	Co $3d_{x2-y2}/3d_{yz}$	cor/ligand-π^*
					110 → 120	10	Co $3d_{yz}/3d_{x2-y2}$	Co $3d_{z2}$/cor-π^*

and significantly lower in energy (note that the x and y axes are rotated by 45° about the z axis from the Co−N(corrin) bond vectors).

Overall, the computed MO diagrams for GSCbl and MeCbl are quite similar, as required by the high resemblance of the experimental GSCbl and MeCbl Abs spectra (Figure 2). One clear difference is that the highest occupied MO (HOMO, MO#124) of GSCbl derives from a lone pair on the S atom of the GS ligand (S_{GS}) that is oriented perpendicular to the Co−S_{GS} bond, whereas the HOMO of MeCbl is corrin π-based. To distinguish between the two S_{GS} lone pairs, the one oriented parallel to the Co−S_{GS} bond will be referred to as the S_{GS} $\pi_{\|}$ orbital and the one oriented perpendicular to the Co−S_{GS} bond as the S_{GS} $\pi_{\perp}$ orbital. Accordingly, it is the S_{GS} $\pi_{\perp}$ orbital that produces the dominant contribution to the HOMO of GSCbl, while the S_{GS} $\pi_{\|}$/Co $3d_{z2}$-based MO#121 is GSCbl's counterpart to the C_{Me} σ/Co $3d_{z2}$-based MO#112 of MeCbl. Note that because the S_{GS} $\pi_{\perp}$ orbital can only engage in "filled/filled" π interactions with occupied Co 3d orbitals, it does not contribute to Co−S_{GS} bonding. The other key difference between the computed MO diagrams for GSCbl and MeCbl is the smaller splitting between the Co−X_{ax} σ-bonding and σ-antibonding MOs in GSCbl, which suggests that the Co $3d_{z2}$/S_{GS} $\pi_{\|}$-bonding interaction is somewhat weaker than the Co $3d_{z2}$/C_{Me} σ-bonding interaction (vide infra).

It is particularly interesting to compare the extent of mixing between the Co $3d_{z2}$ and S_{GS} $\pi_{\|}$ orbitals in GSCbl and between the Co $3d_{z2}$ and the C_{Me} σ orbitals in MeCbl, as this mixing determines the covalency of the Co−X_{ax} bond. The Co−X_{ax} σ-bonding MO of GSCbl (MO#121) has 47% S_{GS} $\pi_{\|}$ and 6% Co $3d_{z2}$ contributions, while the corresponding MO of MeCbl (MO#112) has 36% C_{Me} σ and 15% Co $3d_{z2}$ contributions. The Co $3d_{z2}$-based σ-antibonding counterparts contain 42% Co $3d_{z2}$ and 24% S_{GS} $\pi_{\|}$ contributions in GSCbl (MO#126) and a total of 43% Co $3d_{z2}$ and 28% C_{Me} σ contributions in MeCbl (MOs#119 and #120). A complementary, though less direct measure of the Co−X_{ax} bond covalency is provided by the composition of the highest-energy corrin π-based MO. In GSCbl, this MO (MO#123) has 5% Co $3d_{z2}$ and 9% S_{GS} $\pi_{\|}$ contributions, while the corresponding MO of MeCbl (the HOMO) has 5% Co $3d_{z2}$ and 5% C_{Me} σ contributions. Overall, this analysis of the key MOs of GSCbl and MeCbl reveals that the Co−S_{GS} and Co−C_{Me} bonds are similarly covalent.

(iv). TDDFT-Assisted Spectral Assignments. One notable difference observed in both the experimental and the TDDFT-computed Abs spectra of MeCbl and GSCbl is the apparent red shift of the lowest-energy feature in the latter spectra (Figure 1). The low-energy (α/β) region of the TDDFT-computed GSCbl and MeCbl Abs spectra is shown on an expanded scale in Figure 9, along with electron density difference maps (EDDMs) that illustrate changes in electron density associated with the individual electronic transitions. The lowest-energy electronic transition (band 0) predicted in the GSCbl Abs spectrum has contributions from three distinct one-electron excitations (Table 3), where inspection of the corresponding EDDM (Figure 9) reveals that this transition has primarily S_{GS} $\pi_{\perp}$ → Co 3d/corrin π^* charge transfer character. This transition slightly distorts the TDDFT-computed Abs envelope for GSCbl in the α/β region, giving it a unique low-energy shoulder that is absent in the Abs spectra of alkylcobalamins.

dx.doi.org/10.1021/ic200428r |*Inorg. Chem.* 2011, 50, 8755–8766

Table 3. TDDFT-Calculated Energies (in cm^{-1}), Polarizations, Oscillator Strengths, and Percent Contributions from One-Electron Excitations for the Major Electronic Transitions of GSCbl (band designations relate to Figure 7)

band	state	E (cm^{-1})	polarization	f	transition	%	donor MO	acceptor MO
0	4	17 365	LA	0.0143	123 → 125	23	cor-π (HOMO-1)	cor-π^* (LUMO)
					124 → 126	18	S_{GS}-$\pi_\perp$ (HOMO)	Co $3d_{z2}$/S_{GS}-$\pi_\parallel$ (LUMO+1)
					122 → 126	16	Co $3d_{yz}$/cor-π	Co $3d_{z2}$/S_{GS}-$\pi_\parallel$ (LUMO+1)
i	5	18 136	LA	0.0593	123 → 125	62	cor-π (HOMO-1)	cor-π^* (LUMO)
ii	7	20 465	LA	0.0148	123 → 126	47	cor-π (HOMO-1)	Co $3d_{z2}$/S_{GS}-$\pi_\parallel$ (LUMO+1)
					118 → 128	14	Co $3d_{x2-y2}$	Co $3d_{xy}$
iii	10	23 731	SA	0.0290	122 → 125	54	Co $3d_{yz}$/cor-π	cor-π^* (LUMO)
					123 → 127	34	cor-π (HOMO-1)	cor-π^*
iv	11	24 724	LA	0.0434	121 → 125	54	S_{GS}-$\pi_\parallel$/Co-3d	cor-π^* (LUMO)
v	15	26 343	LA	0.0348	121 → 125	23	S_{GS}-$\pi_\parallel$Co-3d	cor-π^* (LUMO)
					119 → 128	14	Co $3d_{xz}$/cor-π	Co $3d_{xy}$
	16	26 690	SA	0.0331	119 → 125	16	Co $3d_{xz}$/cor-π	cor-π^* (LUMO)
					122 → 128	15	Co $3d_{yz}$/cor-π	Co $3d_{xy}$
					123 → 127	13	cor-π (HOMO-1)	cor-π^*
	17	27 482	SA	0.0407	119 → 125	26	Co $3d_{xz}$/cor-π	cor-π^* (LUMO)
					120 → 125	24	his-π	cor-π^* (LUMO)
					123 → 127	11	cor-π (HOMO-1)	cor-π^*
vi	18	28 198	SA	0.0299	120 → 125	59	his-π	cor-π^* (LUMO)
					119 → 125	20	Co $3d_{xz}$/cor-π	cor-π^* (LUMO)
	19	28 697	SA	0.1194	123 → 127	18	cor-π (HOMO-1)	cor-π^*
					119 → 125	13	Co $3d_{xz}$/cor-π	cor-π^* (LUMO)
					123 → 128	12	cor-π (HOMO-1)	Co $3d_{xy}$
					122 → 125	10	Co $3d_{yz}$/cor-π	cor-π^* (LUMO)

The dominant transition in the α/β region of the TDDFT-computed Abs spectra for both GSCbl and MeCbl (band *i*) primarily involves a one-electron excitation from the highest-energy occupied corrin π-based MO to the lowest-energy unoccupied corrin π^*-based MO, corresponding to the HOMO−1 → LUMO (MO#123 → #125) transition for GSCbl and the HOMO → LUMO transition for MeCbl (MO#116 → #117). The EDDMs associated with these transitions are nearly identical (Figure 9), as are the isosurface plots for the corresponding donor and acceptor MOs (Figure 8). Yet, this transition is predicted to be 125 cm^{-1} lower in energy for GSCbl than for MeCbl, due to the slightly higher energy of the corrin π-based donor MO in the former, consistent with the results from the Gaussian deconvolutions (Table 1, bands 1 and 2). Even though a corrin $\pi \rightarrow \pi^*$ transition is responsible for band *i*, the EDDMs for both GSCbl and MeCbl show a significant loss of electron density in the Co−X_{ax} bonding region (Figure 9), which should weaken this bond in the excited state. This prediction is in excellent agreement with the relatively strong enhancement of ν_{Co-S} and ν_{Co-C} in rR spectra of GSCbl and MeCbl, respectively, obtained with laser excitation into the α/β bands (Figure 4).

The second most intense transition contributing to the α/β region (15 000−22 000 cm^{-1}) of the TDDFT-predicted spectra (band *ii*) is also quite similar in nature for GSCbl and MeCbl. Although this transition is difficult to classify based on the donor and acceptor MOs involved, inspection of the corresponding EDDMs (Figure 9) reveals that in each case significant electron density is transferred from filled Co 3d-based MOs to the empty Co $3d_{z2}$-based MO that also contains a sizable S_{GS} $\pi_\parallel$- or C_{Me} σ-orbital contribution (vide supra).

The γ region (above 26 000 cm^{-1}) of the TDDFT-computed Abs spectrum for GSCbl is dominated by multiple transitions primarily involving corrin $\pi \rightarrow \pi^*$ electronic excitations, though the donor MOs also contain significant Co 3d orbital character (Table 3). Similar transitions are also predicted to occur in the γ region of the MeCbl Abs spectrum (Table 2), albeit with slightly different energies and intensities. In the case of MeCbl, the large number of transitions contributing to the γ region was shown previously to reflect the close energetic proximity of the occupied Co 3d and corrin π-based frontier orbitals.[71] As such, the MeCbl and GSCbl Abs spectra provide an intriguing contrast to the "typical" Co^{3+}Cbl Abs spectra of, for example, H_2OCbl^+ and CNCbl. In H_2OCbl^+ and CNCbl, which lack the strong σ donation from the upper axial ligand found in alkylcobalamins and, as shown here, thiolatocobalamins, the Co 3d-based filled MOs are at much lower energy than the occupied corrin π-based frontier MOs.[71] Alternatively, in GSCbl and MeCbl the strong σ donation from the GS and Me ligands, respectively, greatly lowers the effective nuclear charge of the central Co ion, thereby significantly raising the Co 3d orbitals in energy and enabling extensive mixing with the corrin π-based frontier orbitals. As a result, the γ regions of the alkyl- and thiolatocobalamin Abs spectra have contributions from a large number of transitions with similar energies, leading to the appearance of a broad, weakly structured Abs envelope in this region (Figure 2), while a single sharp feature is observed in the γ region of "typical" Co^{3+}Cbl Abs spectra.[71]

4. DISCUSSION

GSCbl is a physiologically relevant thiolatocobalamin that has recently attracted considerable interest due, in part, to its

dx.doi.org/10.1021/ic200428r |*Inorg. Chem.* 2011, 50, 8755–8766

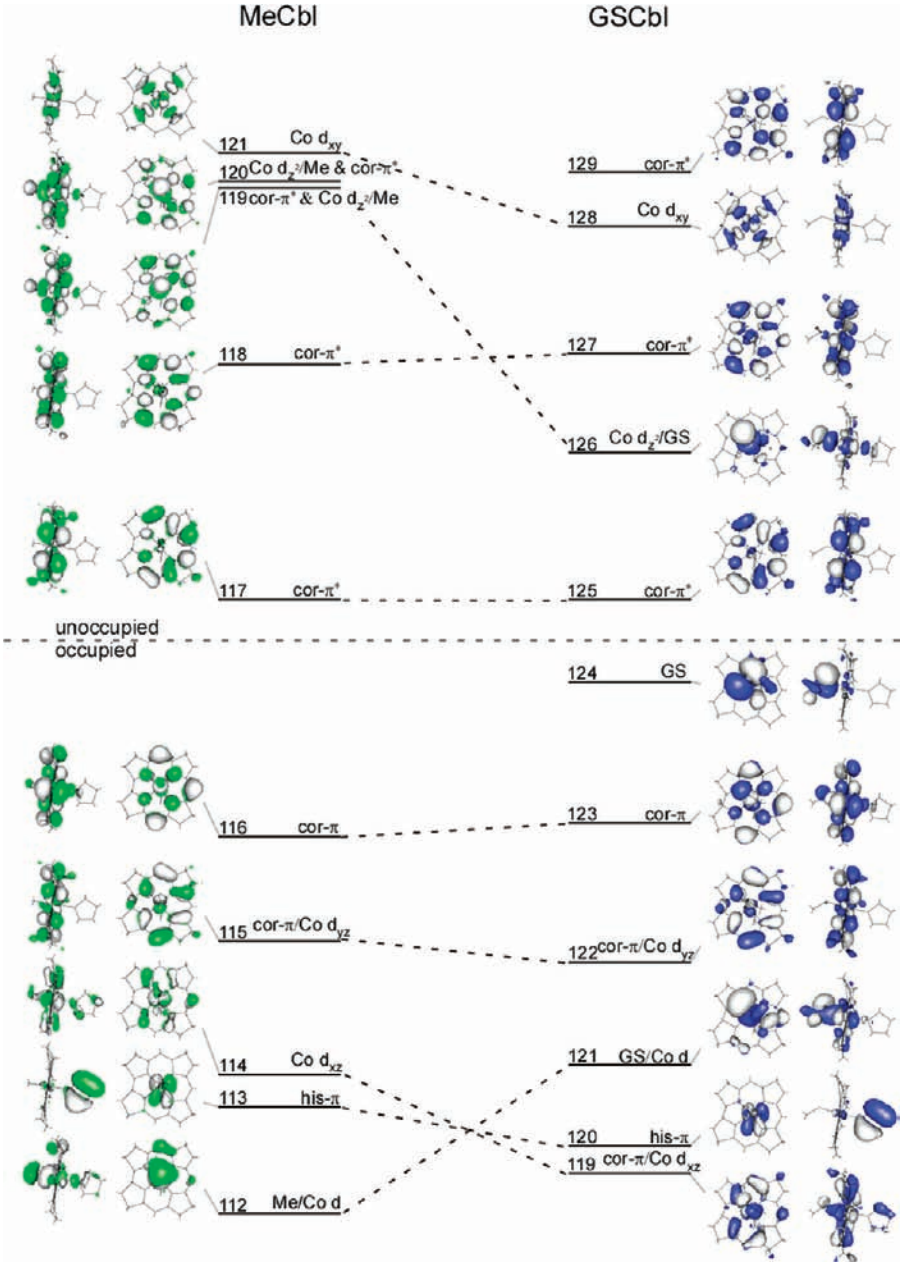

Figure 8. Isosurface plots of the relevant MOs of MeCbl (left) and GSCbl (right). The MOs were shifted vertically to align the LUMOs and are arranged according to their calculated energies with the doubly occupied and unoccupied orbitals shown below and above, respectively, the horizontal dashed line (note that the HOMO/LUMO gap is not drawn to scale).

promise as a treatment for diseases involving oxidative stress.[41,46,48] Importantly, in vitro studies revealed that GSCbl is more effective in protecting cells against oxidative damage than is GSH alone or in combination with any other Cbl. This distinctive behavior of GSCbl has prompted us to investigate its electronic structure, in particular the nature of the Co−S bonding interaction, with a variety of spectroscopic tools. Interestingly, our spectroscopic data reveal striking similarities between GSCbl and MeCbl, a representative member of the family of alkylcobalamins. To corroborate this finding and to develop quantitative electronic structure descriptions for GSCbl and MeCbl, DFT and TDDFT computations were performed on suitably truncated cofactor models. The major findings and implications from these studies are described below.

Axial Ligand Effects on Co^{3+}Cbl Electronic and Vibrational Spectra. The Abs, CD, MCD, and rR spectroscopic data of GSCbl and MeCbl share several common features, which provides direct experimental evidence for the similar natures of the Co−S and Co−C bonding interactions in these species. In each case, the electronic Abs spectrum exhibits low-energy bands associated with corrin $\pi \rightarrow \pi^*$ transitions polarized along the corrin LA and higher-energy features attributable to transitions involving corrin $\pi \rightarrow \pi^*$ and, formally, Co 3d $\rightarrow$ corrin π^* charge transfer excitations polarized along the corrin SA. Moreover, the frequency of the corrin-based ν_{SA} mode, which has been shown to correlate with the charge of the central Co ion,[75] is identical for GSCbl and MeCbl. Nonetheless, our spectral data do reveal small but interesting differences between the electronic structures of GSCbl and MeCbl.

dx.doi.org/10.1021/ic200428r |*Inorg. Chem.* 2011, 50, 8755–8766

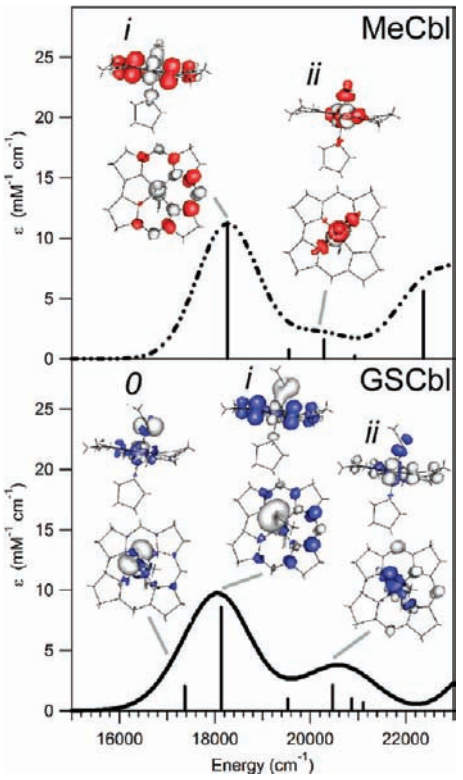

Figure 9. EDDMs for the transitions producing the dominant contributions to the α/β regions of the TDDFT-calculated Abs spectra for MeCbl (top, dashed) and GSCbl (bottom, solid). Blue/red areas designate gain of electron density, and gray areas designate loss of electron density.

Both our spectroscopic and our TDDFT computational results indicate that the β-axial ligation of a thiol instead of an alkyl in Co^{3+} Cbl species causes a small (<500 cm^{-1}) red shift of the lowest-energy Abs feature. Consistent with this finding, our DFT computations predict the corrin π-based MO of GSCbl that serves as the donor orbital in the one-electron transition responsible for the dominant Abs feature in this region to be slightly destabilized in energy from the analogous MeCbl MO (Figure 8, GSCbl MO#123 and MeCbl MO#116). Additionally, our TDDFT results suggest that the α/β region of the GSCbl Abs spectrum actually has contributions from two transitions, in contrast to the single transition responsible for the two low-energy features in this region of the MeCbl Abs spectrum (Figure 9). The lowest-energy band in the GSCbl Abs spectrum, predicted at 16 000 cm^{-1} and possibly observed (though not required in the Gaussian deconvolutions) as a weak low-energy shoulder on the α band, is a diagnostic feature of thiolate ligation, as it corresponds to a S_{GS} $\pi_{\perp}$ → Co 3d/corrin π* charge transfer transition.

Despite small differences in band positions and intensities, the higher-energy γ regions of the experimental GSCbl and MeCbl Abs spectra can be fit with the same number of Gaussian bands. The TDDFT-predicted Abs spectra of GSCbl and MeCbl also share a similar number of bands in this region, where in each case the underlying transitions are of mixed character. The dominant contributors to these bands are corrin π → π* transitions, but Co 3d/S_{GS} or Co 3d/C_{Me} → corrin π* charge transfer transitions also contribute (Tables 2 and 3), which is why the axial ligands modulate the appearance of the Abs envelope in this spectral region.

In the rR spectrum of GSCbl, the Co−S stretch is observed at 325 cm^{-1}, significantly lower in energy than the Co−C stretch of MeCbl, which peaks at 506 cm^{-1} (Figure 4A). This difference can be accounted for largely by the increased mass of the S atom of GS in comparison to the C atom of Me and, thus, does not actually reflect a large difference in Co−S and Co−C bond strengths. Both the Co−S and the Co−C stretches are enhanced with laser excitation into the low-energy Abs feature associated with a corrin π → π* transition (Figure 4), specifically the HOMO−1 → LUMO transition for GSCbl and the HOMO → LUMO transition for MeCbl. Consistent with this experimental finding, our DFT and TDDFT results indicate that the corresponding donor MOs contain a weak σ-bonding interaction between the Co $3d_{z2}$ and S_{GS} $\pi_{\parallel}$/C_{Me} σ orbitals (Figures 8 and 9); hence, removal of an electron from these MOs will weaken the Co−S/Co−C bonds and cause an enhancement of the ν_{Co-S} and ν_{Co-C} modes in the rR spectra of GSCbl and MeCbl, respectively. Another interesting aspect of our rR data is that the ν_{SA} modes of GSCbl and MeCbl have identical frequencies (Figure 5), indicating that the Co^{3+} ions in these two species possess a similar charge and, thus, that the total charge donation from the GS and Me ligands to the Co center is comparable.[75]

Another measure of the axial ligand σ-donor strength is the contribution of the formally unoccupied Co $3d_{z2}$ orbital to the highest-energy corrin π-based MO. Again, this contribution is virtually the same for GSCbl (5.4% in the HOMO-1) and MeCbl (5.2% in the HOMO). The similarities extend to the DFT-calculated Mulliken populations for each species (Table S3, Supporting Information), which predict very similar charges for the α-axial N atoms as well as the two different β-axial ligands. However, the computed charge of the central Co ion is significantly lower in GSCbl than in MeCbl. This difference presumably stems from the increased upper axial ligand−Co bond lengths in the geometry-optimized model of GSCbl but does not actually correlate with our experimental rR data, which indicate that the Co charge is in fact similar in these two species.

Co−S vs Co−C Bonding. The small differences that exist between the GSCbl and the MeCbl spectra indicate that the Co−S and Co−C bonds are slightly different in nature, which is not surprising considering the different energies and compositions of the S_{GS} and C_{Me} frontier orbitals. The HOMO of GSCbl is the S_{GS} $\pi_{\perp}$-based MO that has no counterpart among the MeCbl orbitals. The other occupied frontier MOs with significant axial ligand orbital contributions are the S_{GS} $\pi_{\parallel}$/Co $3d_{z2}$-based MO#121 for GSCbl and C_{Me} σ/Co $3d_{z2}$-based MO#112 for MeCbl (Figure 8). Despite their similar compositions, MO#121 of GSCbl is substantially higher in energy than MO#112 of MeCbl, while the unoccupied Co $3d_{z2}$/S_{GS} $\pi_{\parallel}$-derived σ-antibonding MO of GSCbl is lower in energy than its Co $3d_{z2}$/C_{Me} σ-based counterpart in MeCbl. This finding suggests that the Co $3d_{z2}$/S_{GS} $\pi_{\parallel}$-bonding interaction is somewhat weaker than the Co $3d_{z2}$/C_{Me} σ-bonding interaction, even though the Co−S and Co−C bonds are similarly covalent and the thiolate and alkyl ligands appear to be comparable σ donors to the Co^{3+} center. Notably, the optimized Co−N_{His} bond is 0.061 Å longer in the GSCbl model than in the MeCbl model (Table S2, Supporting Information), which is characteristic of the so-called inverse trans influence previously established for alkylcobalamins.[77]

Implications for GSCbl Function in Vivo. GSCbl forms rapidly under physiological conditions from H_2OCbl^+/HOCbl and GSH (K_f = (1.1 ± 0.3) × 10^5 M^{-1} at 25 °C[43]) and is a fairly stable Cbl, with a measured half-life of its truncated derivative,

dx.doi.org/10.1021/ic200428r |Inorg. Chem. 2011, 50, 8755–8766

γ-glutamylcysteinyl-cobalamin, of ~1.1 × 10^4 min under red light.[42] Since the Co−S and Co−C bonds are quite similar electronically, as revealed by the results obtained in this work, it is easy to conceive how GSCbl may behave similarly as free MeCbl and AdoCbl in the body. Homolytic cleavage of the Co−S bond would result in a free thiyl radical, which has its own aforementioned benefits. With estimates of intracellular Cbls without a protein chaperone at <5%,[26] the possibility that GSCbl would be recognized, absorbed, and imported into the cell remains. Once inside the lysosome, GSCbl could be utilized as a whole or for its two separate parts the GS^- moiety and Co^{3+}Cbl, which have proven to be beneficial in many ways individually.[34,35,46,78−80] The biological relevance of GSCbl is supported by a variety of in vitro studies.[37,42,43] For example, it was shown that methionine synthase more readily uses GSCbl as a cofactor over CNCbl and H_2OCbl^+ as measured by enzyme activity and that GSCbl displays improved conversion over H_2OCbl^+ to AdoCbl and MeCbl under specific reaction conditions.[37,40] It has also recently been shown that the ABC transporter multidrug resistance protein 1 (MRP1) has a role in eukaryotic Cbl export.[81] MRP1 is a membrane efflux transporter that exports free Cbls and exhibits a high affinity for GSCbl, raising the possibility that GSCbl constitutes a significant fraction of free Cbl found intracellularly. However, in vivo studies of GSCbl are still lacking. Thus, with the full scope of the biochemical role of GSCbl still unknown, the electronic structure information obtained in this study provides valuable insight into the nature of Co−S bonding in Cbls and aids in further defining the physiological role of thiolatocobalamins.

■ ASSOCIATED CONTENT

Supporting Information. Cartesian coordinates for all computational models, additional rR spectra spanning larger frequency ranges, tabulated values of computed Mulliken populations, and further information regarding geometry optimizations. This material is available free of charge via the Internet at http://pubs.acs.org.

■ AUTHOR INFORMATION

Corresponding Author

*Phone: (608) 265-9056. Fax: (608) 262-6143. E-mail: brunold@chem.wisc.edu.

■ ACKNOWLEDGMENT

This work was supported by the NSF (CAREER grant MCB-0238530). The authors thank Dr. Frank Neese (Universität Bonn) for a free copy of his ORCA software package.

■ REFERENCES

(1) Abbreviations: Abs, electronic absorption; AdoCbl, 5′-deoxyadenosylcobalamin; B3LYP, Becke's three-parameter hybrid functional for exchange with the Lee−Yang−Parr correlation functional; Cbl, cobalamin; CCD, charge-coupled device; CD, circular dichroism; CysCbl cysteinylcobalamin; DMB, dimethylbenzimidazole; DFT, density functional theory; EDDM, electron density difference map; EPR, electron paramagnetic resonance; GSCbl, glutathionylcobalamin; GSH, glutathione; H_2OCbl^+, aquocobalamin; LA, long axis; MCD, magnetic circular dichroism; MeCbl, methylcobalamin; MetH, methionine synthase; MMCM, methylmalonyl-CoA mutase; MO, molecular orbital; NIR, near-infrared; QM/MM, quantum mechanics/molecular mechanics; rR, resonance Raman; SA, short axis; TDDFT, time-dependent density functional theory.

(2) Rickes, E. L.; Brink, N. G.; Koniuszy, F. R.; Wood, T. R.; Folkers, K. *Science* **1948**, *107*, 396.
(3) Smith, E. L. *Nature (London)* **1948**, *162*, 144.
(4) Smith, E. L.; Parker, L. F. *Proc. Biochem. Soc.* **1948**, *43*, viii.
(5) Banerjee, R., *Chemistry and Biochemistry of B12*; Wiley-Interscience: New York, 1999.
(6) Hodgkin, D. C. P.; Robertson, J. H.; Trueblood, K. N.; Prosen, R. J.; White, J. G. *Nature (London)* **1956**, *176*, 325–328.
(7) Banerjee, R. *Biochemistry* **2001**, *40*, 6191–6198.
(8) Dolphin, D. *B12*; Wiley: New York, 1982.
(9) Kratky, C.; Farber, G.; Gruber, K.; Wilson, K.; Dauter, Z.; Nolting, H. F.; Konrat, R.; Krautler, B. *J. Am. Chem. Soc.* **1995**, *117*, 4654–4670.
(10) Brown, K. L. *Chem. Rev.* **2005**, *105*, 2075–2150.
(11) Walker, L. A.; Shiang, J. J.; Anderson, N. A.; Pullen, S. H.; Sension, R. J. *J. Am. Chem. Soc.* **1998**, *120*, 7286–7292.
(12) Martens, J. H.; Barg, H.; Warren, M. J.; Jahn, D. *Appl. Microbiol. Biot.* **2002**, *58*, 275–285.
(13) Marsh, E. N. G.; Drennan, C. L. *Curr. Opin. Chem. Biol.* **2001**, *5*, 499–505.
(14) Toraya, T. *Cell. Mol. Life Sci.* **2000**, *57*, 106–127.
(15) Champloy, F.; Gruber, K.; Jogl, G.; Kratky, C. *J. Synchrotron Radiat.* **2000**, *7*, 267–273.
(16) Banerjee, R. V.; Frasca, V.; Ballou, D. P.; Matthews, R. G. *Biochemistry* **1990**, *29*, 11101–11109.
(17) Drennan, C. L.; Huang, S.; Drummond, J. T.; Matthews, R. G.; Lidwig, M. L. *Science* **1994**, *266*, 1669–1674.
(18) Banerjee, R. *Chem. Biol.* **1997**, *4*, 175–186.
(19) Leal, N. A.; Olteanu, H.; Banerjee, R.; Bobik, T. A. *J. Biol. Chem.* **2004**, *279*, 47536–47542.
(20) Matthews, R. G. *Acc. Chem. Res.* **2001**, *34*, 681–689.
(21) Thoma, N. H.; Evans, P. R.; Leadlay, P. F. *Biochemistry* **2000**, *39*, 9213–9221.
(22) Mancia, F.; Evans, P. R. *Struct. Fold. Des.* **1998**, *6*, 711–720.
(23) Gerfen, G. J.; Licht, S.; Willems, J. P.; Hoffman, B. M.; Stubbe, J. *J. Am. Chem. Soc.* **1996**, *118*, 8192–8197.
(24) Magnusson, O. T.; Reed, G. H.; Frey, P. A. *Biochemistry* **2001**, *40*, 7773–7782.
(25) Banerjee, R. *ACS Chem. Biol.* **2006**, *1*, 149–159.
(26) Shevell, M. I.; Rosenblatt, D. S. *Can. J. Neurol. Sci.* **1992**, *19*, 472–486.
(27) Chandler, R. J.; Venditti, C. P. *Mol. Genet. Metab.* **2005**, *86*, 34–43.
(28) Moras, E.; Hosack, A.; Watkins, D.; Rosenblatt, D. S. *Mol. Gen. Metab.* **2007**, *90*, 140–147.
(29) Padovani, D.; Gherasim, C.; Banerjee, R. *Curr. Opin. Chem. Biol.* **2009**, *13*, 1–8.
(30) Coelho, D.; Sourmala, T.; Stucki, M.; Lerner-Ellis, J. P.; Rosenblatt, D. S.; Newbold, R. F.; Baumgartner, M. R.; Fowler, B. *N. Engl. J. Med.* **2008**, *358*, 1454–1464.
(31) Rutsch, F.; Gailus, S.; Miousse, I. R.; Sourmala, T.; Sagne, C.; Toliat, M. R.; Nurnberg, G.; Wittkampf, T.; Buers, I.; Sharifi, A.; Stucki, M.; Becker, C.; Baumgartner, M. R.; Robenek, H.; Marquardt, T.; Hohne, W.; Gasnier, B.; Rosenblatt, D. S.; Fowler, B.; Nurnberg, P. *Nat. Genet.* **2009**, *41*, 234–239.
(32) Sen, C. K. *Biochem. Pharmacol.* **1998**, *55*, 1747–1758.
(33) Schafer, F. Q.; Buettner, G. R. *Free Radical Biol. Med.* **2001**, *30*, 1191–1212.
(34) Wu, G.; Fang, Y. Z.; Yang, S.; Lupton, J. R.; Turner, N. D. *J. Nutr.* **2004**, *134*, 489–492.
(35) Pompella, A.; Visvikis, A.; Paolicchi, A.; Tata, V. D.; Casini, A. F. *Biochem. Pharmacol.* **2003**, *66*, 1499–1503.
(36) Zhao, R.; Lind, J.; Merenyi, G.; Eriksen, T. E. *J. Chem. Soc., Perkin Trans. 2* **1997**, 569–574.
(37) Xia, L.; Ballou, D. P.; Marsh, E. N. G. *Biochemistry* **2004**, *43*, 3238–3245.
(38) Ling, X.; Cregan, A. G.; Berben, L. A.; Brasch, N. E. *Inorg. Chem.* **2004**, *43*, 6848–6857.
(39) Wagner, F.; Bernhauer, K. *Ann. N. Y. Acad. Sci.* **1964**, *112*, 580–589.

(40) Pezacka, E.; Green, R.; Jacobsen, D. W. *Biochem. Biophys. Res. Commun.* **1990**, *169*, 443–450.
(41) Hannibal, L.; Axhemi, A.; Glushchenko, A. V.; Moreira, E. S.; Brasch, N. E.; Jacobsen, D. W. *Clin. Chem. Lab. Med.* **2008**, *46*, 1739–1746.
(42) Suto, R. K.; Brasch, N. E.; Anderson, O. P.; Finke, R. G. *Inorg. Chem.* **2001**, *40*, 2686–2692.
(43) Brasch, N. E.; Hsu, T. L. C.; Doll, K. M.; Finke, R. G. *J. Inorg. Biochem.* **1999**, *76*, 197–209.
(44) Adler, N.; Medwick, T.; Poznanski, T. J. *J. Am. Chem. Soc.* **1966**, *88*, 5018–5020.
(45) Nome, F.; Fendler, J. H. *Dalton Trans* **1976**, 1212–1219.
(46) Birch, C. S.; Brasch, N. E.; McCaddon, A.; Williams, J. H. H. *Free Radical Biol. Med.* **2009**, *47*, 184–188.
(47) Kwok, T.; Lee, J.; Lam, L.; Woo, J. *Arch. Gerontol. Geriatr.* **2008**, *46*, 273–282.
(48) McCaddon, A.; Regland, B.; Hudson, P.; Davies, G. *Neurology* **2002**, *58*, 1395–1399.
(49) Randaccio, L.; Furlan, M.; Geremia, S.; Slouf, M.; Srnova, I.; Toffoli, D. *Inorg. Chem.* **2000**, *39*, 3403–3413.
(50) Randaccio, L.; Geremia, S.; Stener, M.; Toffoli, D.; Zangrando, E. *Eur. J. Inorg. Chem.* **2002**, 93–103.
(51) Scheuring, E. M.; Sagi, I.; Chance, M. R. *Biochemistry* **1994**, *33*, 6310–6315.
(52) Randaccio, L.; Geremia, S.; Nardin, G.; Slouf, M.; Srnova, I. *Inorg. Chem.* **1999**, *38*, 4087–4092.
(53) Hannibal, L.; Smith, C. A.; Jacobsen, D. W. *Inorg. Chem.* **2010**, *49*, 9921–9927.
(54) Zheng, D.; Birke, R. L. *J. Am. Chem. Soc.* **2001**, *124*, 9066–9067.
(55) Scheinder, Z.; Stroinski, A., *Comprehensive B12: Chemistry, Biochemistry, Nutrition, Ecology and Medicine*; De Gruyter: New York, 1987.
(56) Fonseca Guerra, C. F.; Snijders, J. G.; te Velde, G.; Baerends, E. J. *Theor. Chem. Acc.* **1998**, *99*, 391–403.
(57) te Velde, G.; Bickelhaupt, F. M.; Baerends, E. J.; Fonseca Guerra, C. F.; van Gisbergen, S. J. A.; Snijders, J. G.; Ziegler, T. *J. Comput. Chem.* **2001**, *22*, 931–967.
(58) Stich, T. A.; Buan, N. R.; Brunold, T. C. *J. Am. Chem. Soc.* **2004**, *126*, 9735–9749.
(59) Vosko, S. H.; Wilk, L.; Nusair, M. *Can. J. Phys.* **1980**, *58*, 1200–1211.
(60) Perdew, J. P.; Burke, K.; Ernzerhof, M. *Phys. Rev. Lett.* **1996**, *77*, 3865–3868.
(61) Neese, F. *ORCA-An ab initio, Density Functional, and Semiempirical Program Package*, Version 2.6.35; Universität Bonn: Bonn, Germany, 2008.
(62) Becke, A. D. *J. Chem. Phys.* **1993**, *98*, 5648–5652.
(63) Becke, A. D. *J. Chem. Phys.* **1993**, *98*, 1372–1377.
(64) Lee, C.; Yang, W.; Parr, R. G. *Phys. Rev. B: Condens. Matter* **1988**, *37*, 785–789.
(65) Schäfer, A.; Huber, C.; Ahlrichs, R. *J. Chem. Phys.* **1994**, *100*, 5829–5835.
(66) Schäfer, A.; Horn, H.; Ahlrichs, R. *J. Chem. Phys.* **1992**, *97*, 2571–2577.
(67) Laaksonen, L. *gOpenMol version 2.32*; Center for Scientific Computing: Espoo, Finland, 2005.
(68) Laaksonen, L. *J. Mol. Graph.* **1992**, *10*, 33–34.
(69) Bergman, D. L.; Laaksonen, L.; Laaksonen, A. *J. Mol. Graph. Model* **1997**, *15*, 301–306.
(70) The computational results obtained with the geometry-optimized MeCbl model are similar to those previously published by this group. The previous computational methodology did not include a geometry optimization of the model from the crystal structure coordinates, and the computations were completed using earlier versions of ADF and ORCA. Thus, the results published here are significantly updated, but the qualitative results and interpretation remain unchanged.
(71) Stich, T. A.; Brooks, A. J.; Buan, N. R.; Brunold, T. C. *J. Am. Chem. Soc.* **2003**, *125*, 5897–5914.
(72) Dong, S.; Padmakumar, R.; Banerjee, R. V.; Spiro, T. G. *J. Am. Chem. Soc.* **1996**, *118*, 9182–9183.
(73) Dong, S.; Padmakumar, R.; Banerjee, R. V.; Spiro, T. G. *Inorg. Chim. Acta* **1998**, *270*, 392–398.
(74) Andruniow, T.; Zgierski, M. Z.; Kozlowski, P. M. *J. Phys. Chem. A* **2002**, *106*, 1365–1373.
(75) Liptak, M. D.; Brunold, T. C. *J. Am. Chem. Soc.* **2006**, *128*, 9144–9156.
(76) *CRC Handbook of Chemistry and Physics*, 91st ed.; CRC Press: Cleveland, OH, 2011.
(77) Andruniow, T.; Zgierski, M. Z.; Kozlowski, P. M. *Chem. Phys. Lett.* **2000**, *331*, 509–512.
(78) Wheatley, C. *J. Nutr. Environ. Med.* **2007**, *16*, 212–226.
(79) Obeid, R.; McCaddon, A.; Herrmann, W. *Clin. Chem. Lab. Med.* **2007**, *45*, 1590–1606.
(80) Herrmann, W.; Obeid, R. *Clin. Chem. Lab. Med.* **2007**, *45*, 1614–1620.
(81) Beedholm-Ebsen, R.; van de Wetering, K.; Hardlei, T.; Nexo, E.; Borst, P.; Moestrup, S. K. *Blood* **2010**, *115*, 1632–1639.